Hydrol. Earth Syst. Sci. Discuss., 9, 261–300, 2012
www.hydrol-earth-syst-sci-discuss.net/9/261/2012/
doi:10.5194/hessd-9-261-2012

Hydrology and Earth System Sciences Discussions

Potential effects of climate change on inundation patterns in the Amazon Basin

F. Langerwisch[1], S. Rost[2], D. Gerten[2], B. Poulter[3], A. Rammig[1], and W. Cramer[1]

[1]Earth System Analysis, Potsdam Institute for Climate Impact Research (PIK), P.O. Box 60 12 03, Telegraphenberg A62, 14412 Potsdam, Germany
[2]Climate Impacts and Vulnerabilities, Potsdam Institute for Climate Impact Research (PIK), P.O. Box 60 12 03, Telegraphenberg A62, 14412 Potsdam, Germany
[3]Laboratoire des Sciences du Climat et l'Environnement (LSCE), Orme des Merisiers, bat. 701 – Point courrier 129, 91191 Gif Sur Yvette, France

Received: 16 December 2011 – Accepted: 22 December 2011 – Published: 6 January 2012

Correspondence to: F. Langerwisch (fanny.langerwisch@pik-potsdam.de)

Published by Copernicus Publications on behalf of the European Geosciences Union.

Abstract

A key factor for the functioning and diversity of Amazonian rain forests is annual flooding. However, increasing air temperature and higher precipitation variability, caused by climate change, are expected to shift the flooding regime, and thereby negatively impact floodplain ecosystems, their biodiversity and riverine ecosystem services during this century. To assess the effects of climate changes on the flooding regime, we use the Dynamic Global Vegetation and Hydrology Model LPJmL, enhanced by a scheme that realistically simulates floodable area and inundation. Regarding hydrograph and inundation area, simulation results under contemporary conditions compare well against observations. The changes of calculated river discharge and inundation, under climate change projections from 24 IPCC AR4 climate models, differ regionally towards the end of the 21st century. Flooded area increases in about one third of the basin, with a probability larger than 70 %. Inundation duration increases dramatically by on average three months in Western and around one month in Eastern Amazonia. The time of high- and low-water-peak shifts by up to three months. We find a slight decrease in the number of extremely dry years as well as a decrease of the probability of the occurrence of three consecutive extremely dry years. The total number of extremely wet years does not change drastically but the probability of three consecutive extremely wet years decreases by up to 30 % in the East and increases by up to 25 % in the West. These changes implicate significant shifts in regional vegetation and climate, and will dramatically alter carbon and water cycles.

1 Introduction

Amazonia plays a vital role for the global water and carbon cycles through enormous water and carbon stores and fluxes. The Amazon catchment covers six million square kilometers and about 15 % of the world's freshwater runoff is discharged by the Amazon River (Gaillardet et al., 1997). Dissolved in this water, about 33 $\mathrm{Tg\,C\,yr^{-1}}$ are thought

HESSD
9, 261–300, 2012

to be exported to the Atlantic Ocean as organic carbon (Moreira-Turcq et al., 2003). A much larger amount, approximately 470 Tg C yr^{-1}, gasses out to the atmosphere as CO_2 (Richey et al., 2002). Climate and land use change currently affect Amazonian forests substantially, leading to a reduction of biomass, biodiversity and ecosystem services (Laurance and Williamson, 2001; Fearnside, 2004; Foley et al., 2007; Nepstad et al., 2007; Betts et al., 2008; Poulter et al., 2009). Since the forcing from changing climate and land use appears to be nonlinearly related to the stability of the Amazonian ecosystem (Sitch et al., 2008; Nobre and De Simone Borma, 2009), this region has been identified as one of a set of global "tipping elements" particularly susceptible to global change (Lenton et al., 2008).

Much of Central Amazonia is influenced by annual flooding caused by snow melt in the Andes and precipitation across the basin. During the flooding season between January and March (Foley et al., 2002) the water rises with an amplitude of 5 to 15 m (Junk, 1985) and an average speed of 0.05 m d^{-1} (Junk and Piedade, 1997). The extent of flooded area in Central Amazonia increases from about 4 % during low water to 16 % during high water stage (Richey et al., 2002). The recurrent change between the terrestrial and aquatic phase forms characteristic and very diverse habitats for millions of plant and animal species. These floodplains are alternately suitable for aquatic and terrestrial organisms. Floodplain forests cover approximately 97 000 km^2 (Parolin et al., 2004) and contain about 20 % of the 4000–5000 Amazonian tree species (Naiman et al., 2005). The vast floodplain areas thus represent one of the riches biota on earth, providing several ecosystem services, such as timber and fish production and carbon storage (Keddy et al., 2009).

Life of plant and animal species is intimately related to the recurrent annual flooding. The distribution of floodplain vegetation is especially influenced by duration of the aquatic and terrestrial phase (Junk and Piedade, 1997). To cope with flooding, plant species developed several adaptation strategies and methods. Morphological adaptations such as lenticels and aerenchyma (Junk and Piedade, 1997; Parolin, 2002; Worbes, 1997) and physiological adaptations such as reduction in photosynthetic

HESSD
9, 261–300, 2012

activity (Junk and Piedade, 1997; Worbes, 1997; Parolin et al., 2004) evolved. In many plant species reproduction, growth and dispersal are triggered by different flood stages (Junk et al., 1989; Worbes, 1997; Junk and Piedade, 1997; Godoy et al., 1999; Parolin, 2002; De Simone et al., 2002). Survival strategies in animals, like in plant species, are also determined by frequency, amplitude and duration of flooding. The animal species are adapted by behavioral (e.g. migration), and physiological (e.g. dormancy) systems (Worbes, 1997; Adis, 1997; Gauer, 1997). Additionally reproduction, growth and dispersal in many animal species are controlled by different flood stages (Junk et al., 1997; Junk and Da Silva, 1997; Adis, 1997).

Climate change is expected to alter temperature and precipitation patterns, which can potentially lead to changes in flood regime such as a reduction in discharge in the Amazon River (Arora and Boer, 2001). The variability in precipitation is expected to increase, causing a higher spatial and temporal variability in river discharge and flooded area (Coe et al., 2002). The effect of climate changes on the El Niño Southern Oscillation (ENSO) remains unclear (Malhi and Wright, 2004) but ENSO changes discharge drastically (Foley et al., 2002). Changes in time, duration, and height of the flood will shift the distribution of vegetation (Cox et al., 2004), potentially causing feedbacks to the atmosphere (Sampaio et al., 2007; Malhi et al., 2008). To understand and quantify the magnitude of impacts of future climate change on the Amazonian water balance, we apply an enhanced process-based model. The model includes the dynamic and spatially explicit reproduction of the specific hydrological patterns of the main river stem and its tributaries. These patterns consist of seasonal discharge, time and duration of low/high water periods and the changing extent of the flooded area during those periods. We use the Dynamic Global Vegetation and Hydrology Model LPJ managed Land (LPJmL), which simulates terrestrial vegetation dynamics in coupling with carbon and water cycles (Sitch et al., 2003; Bondeau et al., 2007; Rost et al., 2008).

Here we describe a new method to calculate flow velocities and inundated area, evaluate our simulated results against observed data, and estimate changes in inundation patterns in Amazonia. Finally, we discuss potential effects of these changes on

HESSD
9, 261–300, 2012

plant and animal species. To estimate the amplitude of changes in the flood regime caused by climate change we use forcing data of the 24 climate models used in the 4th Assessment Report of the Intergovernmental Panel on Climate Change (IPCC, 2007; Randall et al., 2007).

2 Methods

To understand current Amazonian inundation patterns and to assess the effect of climate change on these patterns, we apply the Dynamic Global Vegetation and Hydrology Model LPJmL (Sitch et al., 2003; Gerten et al., 2004; Bondeau et al., 2007; Rost et al., 2008). LPJmL computes establishment, abundance, vegetation dynamics, growth and productivity of the world's major plant functional types, as well as the associated carbon and water fluxes. The model is typically applied on a grid of $0.5^{\circ} \times 0.5^{\circ}$ longitude/latitude and at daily time steps. Carbon fluxes and vegetation dynamics are directly coupled to water fluxes. Modeled soil moisture, runoff and evapotranspiration were found to reproduce observed patterns well and their quality is comparable to stand-alone global hydrological models (Wagner et al., 2003; Gerten et al., 2004, 2008; Gordon et al., 2004; Biemans et al., 2009).

In the river routing module of LPJmL (described by Rost et al., 2008) each grid cell is considered to have a surface water storage pool representing the water storage and retention in reservoirs and lakes. The change of the storage in the river over time is represented as the runoff generated in the cell, the input of discharge accumulated from upstream grid cells, the output to the downstream cell, and the outflow of lakes in the respective cell. The output to the downstream cell is determined as a linear transport of discharge, depending on the flow velocity (v) and the distance between the midpoints of the connected cells. Earlier versions of LPJmL used a globally homogeneous flow velocity of $1\,\mathrm{m\,s^{-1}}$ (Rost et al., 2008), which had difficulties to reproduce the Amazonian hydrograph. In a former study we already improved the reproduction of the hydrograph by applying a homogeneously reduced flow velocity of $0.25\,\mathrm{m\,s^{-1}}$ to the Amazon Basin

HESSD
9, 261–300, 2012

(Langerwisch et al., 2008). But a heterogeneous flow velocity which takes orographic differences within the Amazon catchment into account is more appropriate. Therefore, we develop a method to calculate site specific flow velocities.

2.1 Calculation of flow velocity and floodable area

Here we extend earlier work (Langerwisch et al., 2008) by calculating site specific flow velocities to take slope into account. Additionally, we estimate the extent of flooded area. To calculate the flow velocity and the flooded area we use a digital elevation model (DEM) provided by the WWF database HydroSHEDS (WWF HydroSHEDS, 2007) at a resolution of 15 arcsec longitude/latitude, corresponding to approximately 460 m edge length in the study region. We use grid-based elevation data (instead of elevation data of the actual gauging stations) to have a continuous spatially consistent basis for our calculations. The elevation values in this DEM do represent the top of the canopy and therefore not the actual ground elevation value (see also Anderson et al., 2009), which will be about 30 m below the DEM elevation value. We assume that the difference in the DEM elevation, which we basically use for the flow velocity calculations represent the actual difference in elevation for the site. The following calculations (Sects. 2.1.1 and 2.1.2) were processed at the native resolution of HydroSHEDS. Final results are resampled to a $0.5^{\circ} \times 0.5^{\circ}$ (longitude/latitude) resolution.

2.1.1 Flow velocity

Based on the DEM we calculate the East-West elevation gradient $\delta Z/\delta X$ (Eq. 1) and the North-South elevation gradient $\delta Z/\delta Y$ (Eq. 2) for each cell$_{i,j}$ with i and j defining the cell's spatial position using

$$[\delta Z/\delta X]_{i,j} = \frac{(Z_{i+1,j+1} + 2Z_{i+1,j} + Z_{i+1,j-1}) - (Z_{i-1,j+1} + 2Z_{i-1,j} + Z_{i-1,j-1})}{N \times \delta x} \quad (1)$$

$$[\delta Z/\delta Y]\, i,j = \frac{(Z_{i+1,j+1} + 2Z_{i,j+1} + Z_{i-1,j+1}) - (Z_{i+1,j-1} + 2Z_{i,j-1} + Z_{i-1,j-1})}{N \times \delta y} \quad (2)$$

HESSD
9, 261–300, 2012

where X, Y (radians) are coordinate axes and Z (m) is elevation of the cell$_{i,j}$; $N = 8$ is the number of neighboring cells, δx and δy (m) are the distances between cell centers; $j+1$ and $j-1$ are the adjacent cells to the North and South, respectively and $i+1$ and $i-1$ are the adjacent cells to the East and West, respectively. Values are calculated using a 3×3 cell window.

The calculation of the high resolution slope S (degree) is based on the work of Burrough (1986). Using equation Eqs. (1) and (2) we calculate

$$S = \tan A \sqrt{\left(\frac{\delta Z}{\delta X}\right)^2 + \left(\frac{\delta Z}{\delta Y}\right)^2} \times c \quad (3)$$

with c set to 57.29 to convert from radian to decimal degree. We apply the median of all subcell values to aggregate the high resolution slope to a $0.5^\circ \times 0.5^\circ$ cell slope.

Subsequently we calculate slope dependent flow velocity v (m s^{-1}) (Fig. 1) based on the Manning–Strickler formulation

$$v = I^{1/2} \times k \times R^{2/3} \quad (4)$$

where I is the linear hydraulic head loss (–), a reduction of elevation over certain distance, that directly depends on slope. The Manning–Strickler coefficient k (m$^{1/3}$ s^{-1}) describes the roughness of the area. For natural rivers this value ranges between 30 and 40 (Patt, 2001). Due to the lack of detailed cell specific information we set $k = 35$. Setting $k = 30$ or $k = 40$ would cause a change of the calculated flow velocities of about +10.8 % and −8.5 % in comparison to $k = 35$, respectively. R is the hydraulic radius (m). Since we have no detailed information about the river profile neither in headwater cells nor in main stem cells, we neglected the influence of this factor and set $R = 1$.

2.1.2 Floodable area

As a basis for inundation calculation we estimate potentially floodable area. Applying the same DEM used for the flow velocity calculation (see Sect. 2.1.1) we determine a modified Topographic Relative Moisture Index (mTRMI) based on the work of

HESSD
9, 261–300, 2012

Parker (1982) on the native resolution of the DEM (15 arcsec). This index is applied to classify structural landscape conditions which can be arranged in 7 different landform types, like *valley flats* and *dry steep slopes* (also see Table 3). It uses several weighted geomorphologic characteristics such as slope, slope steepness, slope configuration, relative slope position, and aspect which can be calculated from the DEM. We use the resulting landform type *valley flats* as potentially floodable area.

In this study, the mTRMI is the sum of classified slope, classified slope configuration and classified relative slope position (see below for definitions). We neglect the aspect because differences between North and South facing slopes are insignificant in the tropics (compare to Donnegan et al., 2007). In the following paragraphs we describe the calculation of the mTRMI summands.

The first summand is classified slope. We use the previously calculated slope values and slice them in six slope classes (Table 1).

The second summand is classified slope configuration. Slope configuration describes the convexity or concavity of the land surrounding any grid cell, based on the change in elevation Z (m) from cell$_{i,j}$ to all cells located at the edge of the 5×5 cell window. We determine slope configuration, both diagonally (Eq. 5) and orthogonally (Eq. 6) ($Z_{\mathrm{Mean_{dia}}}$, $Z_{\mathrm{Mean_{ortho}}}$), directly from the DEM.

$$Z_{\mathrm{Mean_{dia}}} = \frac{Z_{i-2,j+2} + Z_{i+2,j+2} + Z_{i-2,j-2} + Z_{i+2,j-2}}{E} \tag{5}$$

$$Z_{\mathrm{Mean_{ortho}}} = \frac{Z_{i,j+2} + Z_{i-2,j} + Z_{i+2,j} + Z_{i,j-2}}{E} \tag{6}$$

with $E = 4$ as the number of edge cells. Since the distance between the target cell and the diagonal corner cells of the window is larger (and its influence is smaller) than the distance between the target cell and the orthogonal edge cells, we weight the influence of the values for the different distances (Eqs. 7 and 8) between the target cell and a cell at the edge of the window depending on the orientation ($Z_{\mathrm{Diff_{dia}}}$, $Z_{\mathrm{Diff_{ortho}}}$).

HESSD
9, 261–300, 2012

$$Z_{\mathrm{Diff}_{\mathrm{dia}}} = 100 \times \frac{Z_{\mathrm{Mean}_{\mathrm{dia}}} - Z_{i,j}}{\delta x_{\mathrm{dia}}} \tag{7}$$

$$Z_{\mathrm{Diff}_{\mathrm{ortho}}} = 100 \times \frac{Z_{\mathrm{Mean}_{\mathrm{ortho}}} - Z_{i,j}}{\delta x_{\mathrm{ortho}}} \tag{8}$$

where δx_{dia} and $\delta x_{\mathrm{ortho}}$ are the distances (m) between cell centers. We calculate the slope configuration as follows.

$$\mathrm{slope}_{\mathrm{config}} = \frac{Z_{\mathrm{Diff}_{\mathrm{dia}}} + Z_{\mathrm{Diff}_{\mathrm{ortho}}}}{2} \tag{9}$$

Afterwards we slice the full range of resulting values equally into 10 parts and assign these parts into 3 slope configuration classes: slices 0–4 to class −1 (convex topography); slice 5 to class 0 (flat topography); slices 6–10 to class 1 (concave topography).

The third summand is relative slope position. It describes the distance of the cell$_{i,j}$ to the closest ridges and streams. To calculate this distance, we determine the flow direction (Eq. 10) by finding the steepest descent from the cell to any of its neighbors

$$\mathrm{flow}_{\mathrm{cell}} = 100 \times \frac{\delta Z}{\delta x} \tag{10}$$

where δZ is the difference in elevation and δx the difference between the cell centers. We code its direction with eight values. The resulting flow direction map is used to compute the flow accumulation which is the number of cells draining into each cell. To define the river network we use all cells to which at least 100 cells drain. Afterwards we reduce the channel width to 1 cell to define the actual riverbed. We then define the ridges by creating a smoothed elevation grid over a 20 × 20 cell window

$$Z_{\mathrm{smooth}} = \left(\sum_{n=-9}^{10} \sum_{m=-9}^{10} Z_{i+n,j+m} \right) \Big/ 400 \tag{11}$$

HESSD
9, 261–300, 2012

in which extraordinary peaks and sinks are removed, and subtracting it from the elevation map. The difference map between the smoothed grid and the elevation grid is used to calculate the ridge lines (difference < 10 m) which are afterwards reduced to 1 cell ridge width to define the actual ridge line. Now the relative distance (cells) between riverbed and ridge is calculated. We assign these values to 6 relative slope position classes (Table 2).

From the slope classes (Eqs. 1–3), the slope configuration classes (Eqs. 5–9) and the relative slope position classes (Eqs. 10–11) we calculate mTRMI. We sum up classified slope (0 to 5), classified slope configuration (−1 to 1), and classified relative slope position (10 to 22). The mTRMI ranges from dry to wet (9 to 28), describing site conditions.

We generate a map (15 arcsec resolution) of landform types by combining slope S and mTRMI. For this purpose we group sites with defined mTRMI and slope to certain landform types (details in Table 3). Finally we use the landform type *valley flat*, which is potentially floodable area, to calculate the fraction (%) of floodable area for each $0.5^{\circ} \times 0.5^{\circ}$ grid cell.

To calculate actual flooded area we first estimate the continuously flooded area (low water river area) per $0.5^{\circ} \times 0.5^{\circ}$ cell. Richey et al. (2002) estimated that during low water about 4 % and during high water 16 % of a 1.77 million km^2 quadrant of the Central Amazon Basin are covered with water. We therefore assume that 25 % of the potential floodable area is continuously covered with water. The actual monthly flooded area is calculated by assuming that under current conditions (reference period 1961–1990) the floodable area is totally covered with water if the maximum annual mean discharge plus the standard deviation for this period is reached. Therefore it is possible that more than the maximal floodable area is flooded during anomalously high water discharge years.

HESSD
9, 261–300, 2012

2.2 Data and simulations

LPJmL (Version 3.4.008) is run in its natural vegetation mode on a 0.5° × 0.5° spatial resolution for the period 1901–2099. The transient runs are preceded by 1000 yr spin up during which the pre-industrial CO_2 level of 280 ppm and the climate of the years 1901–1930 are repeated to obtain equilibrium for vegetation, carbon and water pools.

For the model evaluation we perform model runs using climate forcing data from a homogenized and extended CRU TS2.1 global climate dataset covering the years 1901–2003 (Österle et al., 2003; Mitchell and Jones, 2005). For the projections we take climate forcing data from 24 Coupled General Circulation Models (Table 4) chosen for the 4th Assessment Report of the IPCC (Nakićenović et al., 2000; Meehl et al., 2007) calculated under the SRES A1B scenario. The ability of the different Circulation Models to reproduce the mean and variability of observed South American rainfall was discussed by Jupp et al. (2010). Uncertainties of climate models are discussed by Rowell (2011), with highest uncertainties in the deep tropics, especially over South America. By applying the model results of 24 GCMs we include a wide range of future precipitation and temperature projections, we therefore also include these model uncertainties in our results.

To get quasi-daily values, the monthly values of temperature and cloud cover are linearly interpolated. Daily precipitation amount and distribution of wet days are inferred using a stochastic method (Gerten et al., 2004). To remove climate bias from the IPCC AR4 climate scenarios, we conduct an anomaly approach to standardize the climate input for LPJmL (see also Rammig et al., 2010). For Southern Amazonia a decrease of precipitation is expected by the end of the century (especially during the Southern Hemisphere winter), whereas an increase in precipitation is expected in the Northern part. The temperature is projected to increase by about 3.5° (Meehl et al., 2007). Soil information is derived from the FAO global database (FAO, 1991; Sitch et al., 2003).

HESSD
9, 261–300, 2012

2.3 Model evaluation and projections

We compare monthly observed discharge from the "River Discharge Database" of the *Center for Sustainability and the Global Environment* (2007) with simulated discharge at 45 sites. For evaluation we use two indices, the Willmott's Index of Agreement, ranging from 0 to 1, with 1 indicating complete agreement (Willmott, 1982) and the Error of the Qualitative Validation, ranging from 0 to infinite, with low values indicating good agreement (Jachner et al., 2007).

For three observation sites (Cruzeiro do Sul, Porto Velho and Óbidos) we show the agreement between observed and modeled discharge in more detail. Cruzeiro do Sul, a low discharge site, is situated in the Western part of the basin 400 km East of the Andes, at an altitude of about 200 m on the Rio Jurua. Porto Velho, a medium discharge site, is situated in Southern Amazonia at an altitude of about 50 m, directly on the large Amazon tributary Rio Madeira. Óbidos is the final gauging station upstream of the estuary (700 km West of the mouth) at an altitude of about 40 m with a very high discharge (details in Table 5, positions indicated in Fig. 1). Additionally we compare the calculated floodable area with published values of floodplain area for 3 subregions of the basin (Hamilton et al., 2002; Melack et al., 2004; Richey et al., 2002; details in Table 6 and Fig. 5).

After evaluating the model for current conditions we analyze future changes in inundation patterns. We compare inundated area, duration of inundation, and high and low water peak month from a 30 yr reference period (1961–1990) with data from the last 30 model years 2070–2099. Furthermore, we extend our analysis to identify change in frequency of extreme events (i.e. droughts and very high floods). We define an event as extreme flood if the flooded area is larger than the 30 yr median flooded area added by the standard deviation (for the considered time period). We define an event as extreme drought if the flooded area is smaller than the mean flooded area reduced by the standard deviation. We calculate probabilities for certain events by combining results of the 24 different model runs. If all model runs (24/24) show this event the probability is 100 %, and 4 % if only one model run shows this event.

HESSD
9, 261–300, 2012

3 Results and discussion

3.1 Current conditions

We first discuss the quality of simulated flow velocity, discharge and flooded area, since these are preconditions for estimating future changes in inundation patterns.

Flow velocity is highest in the Andean region, where the slopes are steepest and lowest in the depression of the basin (Fig. 1). Both the Guiana Highlands and the Brazilian Highlands (Northwest and South of the mouth, respectively) can be identified with a slightly higher velocity than the lowland. For the three selected sites Cruzeiro do Sul, Porto Velho and Óbidos we calculate flow velocities of 0.25 m s^{-1}, which are in good agreement with those reported by Birkett et al. (2002) and Richey et al. (1989) who measured a velocity of 0.35 ± 0.05 and 0.3 m s^{-1}, respectively. The calculated values are slightly lower than the observed values because our model input velocities are calculated using slope medians over 0.5° × 0.5° cells and thereby steep and plane areas are combined. Due to the upscaling of high resolution information to 0.5° × 0.5° cells, we lost the small-scale orography of the river network, but the resulting flow velocity and discharge show good agreement with observations (Figs. 2–4). Therefore the usage of low-resolution information can be considered as appropriate for this study.

The simulated discharge reproduces observed patterns very well. The comparison of the actual river network with the simulated discharge shows very good agreement (Fig. 2). The characteristics of the simulated hydrograph, such as time and height of high and low water phase agree with observed hydrographs (Fig. 3). In our work we simulate the discharge for sites with less than 10 m^3 s^{-1} as well as sites with more than 100 000 m^3 s^{-1} mean June discharge (see Fig. 2). Concerning this wide range of discharge within the basin, the reproduction of the overall discharge pattern is appropriate and unprecedented for a model with predictive capacity. We reproduce the order of magnitude of discharge and regarding the standard deviation of the observed discharge we see that our model results can reproduce the discharge in low, medium and high discharge sites. Nevertheless we do see differences in high and low water

HESSD
9, 261–300, 2012

peak month (e.g. Fig. 3a), but these differences are comparatively small. In our further analysis of shifts of high and low water peak months due to climate change we compare the simulated peak month during a reference period with simulated peak months during a future period. We are therefore confident that the small deviations to earlier peak month in the model will not affect the calculated differences between reference and future period.

For the comparison for all 45 gauging stations we calculated the Willmott's Index of Agreement and the Error of the Qualitative Validation. Both indices show for most of the sites a high agreement between simulated and observed discharge. The Willmott's Index of Agreement is larger than 0.5 in 80 % of all 45 sites (Fig. 4a). For the three selected sites Cruzeiro do Sul, Porto Velho, and Óbidos this index is 0.88, 0.93, and 0.89, respectively. The Error of the Qualitative Validation is smaller than 1.0 in 90 % of all 45 sites (Fig. 4b). For the selected sites this value is 0.26, 0.09, and 0.99, respectively. For this analysis the model was run in its natural vegetation mode. It is known that deforestation changes the hydrological flows e.g. due to changes in surface runoff (Foley et al., 2007). This might lead to small differences between observed and simulated discharge.

The comparison of calculated floodable area with published values for floodplain area shows good spatial agreement. Cells with a high fraction of floodable area are concentrated along the main stems of the river network (Fig. 5). In addition to the Amazon main stem, a large potentially floodable area is calculated in the South of the region (around 15° S, 65° W), realistically reproducing the Llanos de Moxos wetland (upper Rio Madeira Basin). This vast area of about 150 000 km^2 is inundated annually for 3–4 months (Hamilton et al., 2002). According to Melack et al. (2004) about 14 % of the whole Amazon Basin is floodable, this agrees with our result of 12.6 %. Detailed comparison with published data for 3 subregions of the basin (rectangles R1–R3 in Fig. 5) with Hamilton et al. (2002), Richey et al. (2002) and Melack et al. (2004) shows that calculated and observed values are in comparable range for 3 of the 4 regions (Fig. 5, Table 6). In the central basin (R1 and R2 in Fig. 5) our values of floodable

HESSD
9, 261–300, 2012

area are close to observed values. For R1 the value is in between reported values. We underestimate by 17.4 % compared to Richey et al. (2002), and we overestimate by 26 % compared to Melack et al. (2004). For R2, also situated in Central Amazonia we underestimate by 6 % in comparison to Hamilton et al. (2002). Bigger differences were found for the Llanos de Moxos (R3). Here we underestimate the floodable area by about 46 % compared to Hamilton et al. (2002). However, he and his colleagues examine only the Llanos de Moxos, while our rectangular region also includes parts outside this area. Thus, our underestimation of the floodable area in this region is probably a result of the comparison of two slightly different spatial subsets.

To estimate changes in inundation pattern from 1961–1990 compared to projections in 2070–2099 the reproduction of observed hydrograph and floodable area is crucial. As shown above, with our approach of slope dependent flow velocity we can realistically reproduce the hydrograph. This approach can also be applied to various river catchments where a digital elevation model is available. It is especially useful for large catchments where measured values are insufficiently available. Besides this, we can also reasonably reproduce floodable area with the approach of the modified TRMI. This is a basis to calculate actual inundated area, which enables us to estimate the extent of the area of strong interactions between land and river, as this land-river-interface is of importance for plant and animal diversity.

3.2 Future inundation patterns

After showing that the approach can be used to reproduce observed hydrographs and inundation patterns, the investigations were extended to estimate future changes. We identify several spatial and temporal shifts in the inundation regime. For the Western part of Amazonia the probability of an increase in inundated area is very high ranging from 60–100 % (Fig. 6a). For the Eastern part there is no clear trend, about half of the model runs project an increase and half show a decrease in inundation area with probabilities of 50–60 % and 40–60 %, respectively (Fig. 6b). Inundation tends to be lengthened by 2 to 3 months in the Western basin, while in the East a shortening of the

HESSD
9, 261–300, 2012

inundation duration is likely to occur on average by 0.5–1 months (Fig. 7). Furthermore our results indicate that in the North-West temporal shifts in the time of high and low water peak month will occur (Fig. 8). But the exact spatial and temporal dimensions of these changes remain unclear. We calculate a probability of 40–50 % (Fig. 8a) for a 3-months-forwards-shift of the high water peak month in some parts of North-Western Amazonia. There is a similar probability for a 3-months-backwards-shift in other parts of this region (Fig. 8b). A similar pattern can be seen for the low water peak month (Fig. 8c,d).

The analysis of extreme years reveals that in a 30 yr period the quantity of extremely dry years decreases by up to 3 yr in North-West and South-East Amazonia (Fig. 9a). The probability of 3 consecutive dry years decreases in most parts of Amazonia by 30–90 %, with an especially pronounced decrease in North-East and South-West Amazonia (Fig. 10a). Thus dry years are expected to occur less often and more discrete, leading to less predictable conditions. The analysis of extreme wet years shows changes in the quantity with an amplitude of −1.5 to +1.5 yr (Fig. 9b) in a 30 yr period with no clear spatial pattern. The probability for 3 consecutive years with extreme floods shows spatial differences. It decreases by up to 70 % in the East, and it increases by up to 40 % in the North-West (Fig. 10b). The extreme wet years persist longer in the West and are expected to occur more discrete in Eastern Amazonia.

4 Conclusions

Our projections show extensive changes in the inundation patterns towards the end of the century which are mainly due to changes in precipitation patterns (Malhi et al., 2008; Rammig et al., 2010). Modifications in flooded area and inundation duration as well as high and low water peak months and extreme years are likely to occur. Already in this decade, three years with extraordinary water amounts took place (Marengo et al., 2008, 2011; Nobre and De Simone Borma, 2009). The “Core Amazon” (Killeen and Solorzano, 2008), the North-Western part of the Amazon Basin experiences in our

HESSD
9, 261–300, 2012

simulations most of these changes. An increase in inundated area, a lengthening of inundation duration, changes in low and high water peak month combined with shifts in occurrence and duration of extreme events have the potential to change this region substantially. The large-scale changes in floodplain patterns found in this study may amplify projected climate and land use change effects. We assume that the shifted flooding situation will influence several plant and animal species. This will lead to changes in species composition due to shifts in competition and food web networks. Since the biodiversity increases from East to West in the Amazon Basin (Worbes, 1997; ter Steege et al., 2003) the predicted changes in the North-Western part will influence an area with a large and valuable species pool.

The projected changes in inundation will lead to large-scale changes in water and carbon fluxes. The reduction of terrestrial evapotranspiration caused by an increase of inundated area and projected deforestation could lead to a reduced recycling of precipitation and further amplify drought conditions. The South American Low Level Jet is transporting atmospheric moisture from the Amazon southwards to the Parana-La Plata Basin (Marengo et al., 2009). A reduction of moisture in Amazonia might therefore reduce the precipitation of the entire region of South America. The outgassing CO_2 from the Amazon Basin, which is currently estimated to be about 470 Tg C yr^{-1} (Richey et al., 2002), is likely to increase due to longer inundation in the West. The less pronounced shortening of inundation in the East might not be sufficiently able to balance the additional flux. Changes in regional climate will significantly change vegetation patterns in Amazonia and may cause additional carbon emissions. We conclude that changes in inundation patterns caused by climate change will significantly alter the highly complex system in the Amazon Basin.

Acknowledgements. We thank "Pakt für Forschung der Leibniz-Gemeinschaft" for funding the TRACES project. We also thank John Lowry from Utah State University for providing AML script templates to calculate mTRMI and landform types. We thank Heike Zimmermann-Timm, Pia Parolin and Florian Wittmann for fruitful discussion. We also thank the anonymous reviewers for their helpful remarks. Finally we thank our LPJmL and Amazon Group colleagues at PIK.

HESSD
9, 261–300, 2012

References

Adis, J.: Terrestrial invertebrates: survival strategies, group spectrum, dominance and activity patterns, in: The Central Amazon Floodplain, edited by: Junk, W. J., Springer, Berlin, Germany, 299–317, 1997.

Anderson, L. O., Malhi, Y., Ladle, R. J., Aragão, L. E. O. C., Shimabukuro, Y., Phillips, O. L., Baker, T., Costa, A. C. L., Espejo, J. S., Higuchi, N., Laurance, W. F., López-González, G., Monteagudo, A., Núñez-Vargas, P., Peacock, J., Quesada, C. A., and Almeida, S.: Influence of landscape heterogeneity on spatial patterns of wood productivity, wood specific density and above ground biomass in Amazonia, Biogeosciences, 6, 1883–1902, doi:10.5194/bg-6-1883-2009, 2009.

Arora, V. K. and Boer, G. J.: Effects of simulated climate change on the hydrology of major river basins, J. Geophys. Res.-Atmos., 106, 3335–3348, 2001.

Bendix, J. and Hupp, C. R.: Hydrological and geomorphological impacts on riparian plant communities, Hydrol. Process., 14, 2977–2990, 2000.

Betts, R. A., Malhi, Y., and Roberts, J. T.: The future of the Amazon: new perspectives from climate, ecosystem and social sciences, Philos. T. Roy. Soc. B, 363, 1729–1735, doi:10.1098/rstb.2008.0011, 2008.

Biemans, H., Hutjes, R. W. A., Kabat, P., Strengers, B. J., Gerten, D., and Rost, S.: Effects of Precipitation Uncertainty on Discharge Calculations for Main River Basins, J. Hydrometeorol., 10, 1011–1025, doi:10.1175/2008jhm1067.1, 2009.

Birkett, C. M., Mertes, L. A. K., Dunne, T., Costa, M. H., and Jasinski, M. J.: Surface water dynamics in the Amazon Basin: application of satellite radar altimetry, J. Geophys. Res.-Atmos., 107, 26/1–26/21, doi:10.1029/2001JD000609, 2002.

Bondeau, A., Smith, P. C., Zaehle, S., Schaphoff, S., Lucht, W., Cramer, W., Gerten, D., Lotze-Campen, H., Müller, C., Reichstein, M., and Smith, B.: Modelling the role of agriculture for the 20th century global terrestrial carbon balance, Global Change Biol., 13, 679–706, doi:10.1111/j.1365-2486.2006.01305.x, 2007.

Burrough, P. A.: Digital elevation models, in: Principles of Geographical Information Systems for Land Resources Assessment, edited by: Burrough, P. A., Oxford University Press, New York, 39–55, 1986.

Center for Sustainability and the Global Environment (SAGE): River Discharge Database, avasilable at: http://www.sage.wisc.edu/riverdata, last access: 12 October 2007.

HESSD
9, 261–300, 2012

Coe, M. T., Costa, M. H., Botta, A., and Birkett, C.: Long-term simulations of discharge and floods in the Amazon Basin, J. Geophys. Res.-Atmos., 107, 8044, doi:10.1029/2001JD000740, 2002.
Cox, P. M., Betts, R. A., Collins, M., Harris, P. P., Huntingford, C., and Jones, C. D.: Amazonian forest dieback under climate-carbon cycle projections for the 21st century, Theor. Appl. Climatol., 78, 137–156, doi:10.1007/s00704-004-0049-4, 2004.
De Simone, O., Muller, E., Junk, W. J., and Schmidt, W.: Adaptations of Central Amazon tree species to prolonged flooding: root morphology and leaf longevity, Plant Biol., 4, 515–522, 2002.
Donnegan, J. A., Butler, S. L., Kuegler, O., Stroud, B. J., Hiserote, B. A., and Rengulbai, K.: Palau's forest resources, 2003, in: Resour. Bull. PNW-RB-252, US Department of Agriculture, Forest Service, Pacific Northwest Research Station, Portland, OR, p.52, 2007.
FAO: The digitized soil map of the world (Release 1.0), Food and Agriculture Organization of the United Nations, Rome, Italy, 1991.
Fearnside, P. M.: Are climate change impacts already affecting tropical forest biomass?, Global Environ. Change, 14, 299–302, doi:10.1016/j.gloenvcha.2004.02.001, 2004.
Foley, J. A., Botta, A., Coe, M. T., and Costa, M. H.: El Niño – southern oscillation and the climate, ecosystems and rivers of Amazonia, Global Biogeochem. Cy., 16, 79/1–79/17, doi:10.1029/2002GB001872, 2002.
Foley, J. A., Asner, G. P., Costa, M. H., Coe, M. T., DeFries, R., Gibbs, H. K., Howard, E. A., Olson, S., Patz, J., Ramankutty, N., and Snyder, P.: Amazonia revealed: forest degradation and loss of ecosystem goods and services in the Amazon Basin, Front. Ecol. Environ., 5, 25–32, doi:10.1890/1540-9295(2007)5[25:ARFDAL]2.0.CO;2, 2007.
Gaillardet, J., Dupré, B., Allègre, C. J., and Négrel, P.: Chemical and physical denudation in the Amazon River Basin, Chem. Geol., 142, 141–173, 1997.
Gauer, U.: Collembola in Central Amazon inundation forests – strategies for surviving floods, Pedobiologia, 41, 69–73, 1997.
Gerten, D., Schaphoff, S., Haberlandt, U., Lucht, W., and Sitch, S.: Terrestrial vegetation and water balance – hydrological evaluation of a dynamic global vegetation model, J. Hydrol., 286, 249–270, doi:10.1016/j.jhydrol.2003.09.029, 2004.
Gerten, D., Rost, S., von Bloh, W., and Lucht, W.: Causes of change in 20th century global river discharge, Geophys. Res. Lett., 35, L20405, doi:L20405 10.1029/2008gl035258, 2008.

HESSD
9, 261–300, 2012

Godoy, J. R., Petts, G., and Salo, J.: Riparian flooded forests of the Orinoco and Amazon basins: a comparative review, Biodivers. Conserv., 8, 551–586, 1999.
Gordon, W. G., Famiglietti, J. S., Fowler, N. L., Kittel, T. G. F., and Hibbard, K. A.: Validation of Simulated Runoff from Six Terrestrial Ecosystem Models: Results from the VEMAP, Ecol. Appl., 14, 527–545, doi:10.1890/02-5287, 2004.
Hamilton, S. K., Sippel, S. J., and Melack, J. M.: Comparison of inundation patterns among major South American floodplains, J. Geophys. Res.-Atmos., 107, 5/1–5/14, doi:10.1029/2000JD000306, 2002.
Hughes, F. M. R.: Floodplain biogeomorphology, Prog. Phys. Geogr., 21, 501–529, 1997.
IPCC: Climate Change 2007: The Physical Science Basis. Contribution of Working Group I to the Fourth Assessment Report of the Intergovernmental Panel on Climate Change, edited by: Solomon, S., Qin, D., Manning, M., Chen, Z., Marquis, M., Averyt, K. B., Tignor, M., and Miller, H. L., Cambrigde University Press, Cambrigde, UK and New York, NY, USA, available at: http://www.ipcc.ch/publications_and_data/ar4/wg1/en/contents.html, 2007.
Jachner, S., van den Boogaart, K. G., and Petzoldt, T.: Statistical methods for the qualitative assessment of dynamic models with time delay (R package qualV), J. Stat. Softw., 22, 1–30, 2007.
Junk, W. J.: The Amazon floodplain – a sink or source for organic carbon?, Mitt. Geolog.-Palaeont. Inst. Uni. Hamburg, 58, 267–283, 1985.
Junk, W. J. and Da Silva, V. M. F.: Mammals, reptiles and amphibians, in: The Central Amazon Floodplain, edited by: Junk, W. J., Springer, Berlin, Germany, 409–417, 1997.
Junk, W. J. and Piedade, M. T. F.: Plant life in the floodplain with special reference to herbaceous plants, in: The Central Amazon Floodplain, edited by: Junk, W. J., Springer, Berlin, Germany, 147–185, 1997.
Junk, W. J., Bayley, P. B., and Sparks, R. E.: The flood pulse concept in river-floodplain systems, in: Proceedings of the International Large River Symposium, edited by: Dodge, D. P., Can. Spec. Publ. Fish. Aquat. Sci., 106, 110–127, 1989.
Junk, W. J., Soares, M. G. M., and Saint-Paul, U.: The fish, in: The Central Amazon Floodplain, edited by: Junk, W. J., Springer, Berlin, Germany, 385–408, 1997.
Jupp, T. E., Cox, P. M., Rammig, A., Thonicke, K., Lucht, W., and Cramer, W.: Development of probability density functions for future South American rainfall, New Phytol., 187, 682–693, doi:10.1111/j.1469-8137.2010.03368.x, 2010.

HESSD
9, 261–300, 2012

Keddy, P. A., Fraser, L. H., Solomeshch, A. I., Junk, W. J., Campbell, D. R., Arroyo, M. T. K., and Alho, C. J. R.: Wet and wonderful: the world's largest wetlands are conservation priorities, Bioscience, 59, 39–51, doi:10.1525/bio.2009.59.1.8, 2009.

Killeen, T. J. and Solorzano, L. A.: Conservation strategies to mitigate impacts from climate change in Amazonia, Philos. T. Roy. Soc. B, 363, 1881–1888, doi:10.1098/rstb.2007.0018, 2008.

Langerwisch, F., Rost, S., Poulter, B., Zimmermann-Timm, H., and Cramer, W.: Assessing carbon dynamics in Amazonia with the dynamic global vegetation model LPJmL – discharge evaluation, Verh. Internat. Verein. Limnol., 30, 455–458, 2008.

Laurance, W. F. and Williamson, G. B.: Positive feedbacks among forest fragmentation, drought, and climate change in the Amazon, Conserv. Biol., 15, 1529–1535, 2001.

Lenton, T. M., Held, H., Kriegler, E., Hall, J. W., Lucht, W., Rahmstorf, S., and Schellnhuber, H. J.: Tipping elements in the Earth's climate system, P. Natl. Acad. Sci. USA, 105, 1786–1793, doi:10.1073/pnas.0705414105, 2008.

Leyer, I.: Predicting plant species' responses to river regulation: the role of water level fluctuations, J. Appl. Ecol., 42, 239–250, doi:10.1111/j.1365-2664.2005.01009.x, 2005.

Malhi, Y. and Wright, J.: Spatial patterns and recent trends in the climate of tropical rainforest regions, Philos. T. Roy. Soc. B, 359, 311–329, doi:10.1098/rstb.2003.1433, 2004.

Malhi, Y., Roberts, J. T., Betts, R. A., Killeen, T. J., Li, W., and Nobre, C. A.: Climate Change, Deforestation, and the Fate of the Amazon, Science, 319, 169–172, 2008.

Malhi, Y., Aragao, L., Galbraith, D., Huntingford, C., Fisher, R., Zelazowski, P., Sitch, S., McSweeney, C., and Meir, P.: Exploring the likelihood and mechanism of a climate-change-induced dieback of the Amazon rainforest, P. Natl. Acad. Sci. USA, 106, 20610–20615, doi:10.1073/pnas.0804619106, 2009.

Marengo, J., Nobre, C. A., Betts, R. A., Cox, P. M., Sampaio, G., and Salazar, L.: Global Warming and Climate Change in Amazonia: Climate-Vegetation Feedback and Impacts on Water Resources, in: Amazonia and Global Change, edited by: Keller, M., Bustamante, M., Gash, J., and Silva Dias, P., American Geophysical Union, Washington, 273–292, 2009.

Marengo, J. A., Nobre, C. A., Tomasella, J., Cardoso, M. F., and Oyama, M. D.: Hydro-climatic and ecological behaviour of the drought of Amazonia in 2005, Philos. T. Roy. Soc. B, 363, 1773–1778, doi:10.1098/rstb.2007.0015, 2008.

HESSD
9, 261–300, 2012

Marengo, J. A., Tomasella, J., Alves, L. M., and Soares, W. R.: The drought of 2010 in the context of historicaldroughts in the Amazon region, Geophys. Res. Lett., 38, L12703, doi:10.1029/2011GL047436, 2011.

Meehl, G. A., Stocker, T. F., Collins, W. D., Friedlingstein, P., Gaye, A. T., Gregory, J. M., Kitoh, A., Knutti, R., Murphy, J. M., Noda, A., Raper, S. C. B., Watterson, I. G., Weaver, A. J., and Zhao, Z.-C.: Global climate projections, in: Climate Change 2007: The Physical Science Basis, Contribution of Working Group I to the Fourth Assessment Report of the Intergovernmental Panel on Climate Change, edited by: Solomon, S., Qin, D., Manning, M., Chen, Z., Marquis, M., Averyt, K. B., Tignor, M., and Miller, H. L., 2007.

Melack, J. M., Hess, L. L., Gastil, M., Forsberg, B. R., Hamilton, S. K., Lima, I. B. T., and Novo, E. M. L.: Regionalization of methane emissions in the Amazon Basin with microwave remote sensing, Global Change Biol., 10, 530–544, doi:10.1111/j.1529-8817.2003.00763.x, 2004.

Mitchell, T. D. and Jones, P. D.: An improved method of constructing a database of monthly climate observations and associated high-resolution grids, Int. J. Climatol., 25, 693–712, doi:10.1002/joc.1181, 2005.

Moreira-Turcq, P., Seyler, P., Guyot, J. L., and Etcheber, H.: Exportation of organic carbon from the Amazon River and its main tributaries, Hydrol. Process., 17, 1329–1344, doi:10.1002/hyp.1287, 2003.

Naiman, R. J., Décamps, H., and McClain, M. E.: Riparia: Ecology, Conservation, and Management of Streamside Communities, 2005.

Nakićenović, N., Davidson, O., Davis, G., Grübler, A., Kram, T., Lebre La Rovere, E., Metz, B., Morita, T., Pepper, W., Pitcher, H., Sankovski, A., Shukla, P., Swart, R., Watson, R., and Dadi, Z.: IPCC Special Report on Emission Scenarios, available at: http://www.ipcc.ch/ipccreports/sres/emission/index.php?idp=0, 2000.

Nepstad, D. C., Tohver, I. M., Ray, D., Moutinho, P., and Cardinot, G.: Mortality of large trees and lianas following experimental drought in an Amazon forest, Ecology, 88, 2259–2269, doi:10.1890/06-1046.1, 2007.

Nobre, C. A. and De Simone Borma, L.: "Tipping points" for the Amazon forest, Curr. Opin. Environ. Sustain., 1, 28–36, doi:10.1016/j.cosust.2009.07.003, 2009.

Österle, H., Gerstengarbe, F. W., and Werner, P. C.: Homogenisierung und Aktualisierung des Klimadatensatzes des Climate Research Unit der Universität of East Anglia, Norwich, 6. Deutsche Klimatagung 2003 Potsdam, Germany, Terra Nostra 2003, 326–329, 2003.

HESSD
9, 261–300, 2012

Parker, A. J.: The topographic relative moisture index: an approach to soil-moisture assessment in mountain terrain, Phys. Geogr., 3, 160–168, 1982.
Parolin, P.: Life history and environment of *Cecropia latiloba* in Amazonian floodplains, Rev. Biol. Trop., 50, 531–545, 2002.
Parolin, P., De Simone, O., Haase, K., Waldhoff, D., Rottenberger, S., Kuhn, U., Kesselmeier, J., Kleiss, B., Schmidt, W., Piedade, M. T. F., and Junk, W. J.: Central Amazonian floodplain forests: tree adaptations in a pulsing system, Bot. Rev., 70, 357–380, 2004.
Patt, H.: Hochwasser-Handbuch – Auswirkungen und Schutz, Springer Verlag, Berlin, 2001.
Poulter, B., Aragão, L., Heyder, U., Gumpenberger, M., Heinke, J., Langerwisch, F., Rammig, A., Thonicke, K., and Cramer, W.: Net biome production of the Amazon Basin in the 21st century, Glob. Change Biol., 16, 2062–2075, doi:10.1111/j.1365-2486.2009.02064.x, 2009.
Rammig, A., Jupp, T., Thonicke, K., Tietjen, B., Heinke, J., Ostberg, S., Lucht, W., Cramer, W., and Cox, P.: Estimating the risk of Amazonian forest dieback, New Phytol., 187, 694–706, doi:10.1111/j.1469-8137.2010.03318.x, 2010.
Randall, D. A., Wood, R. A., Bony, S., Colman, R., Fichefet, T., Fyfe, J., Kattsov, V., Pitman, A., Shukla, J., Srinivasan, J., Stouffer, R. J., Sumi, A., and Taylor, K. E.: Climate models and their evaluation, in: Climate Change 2007: The Physical Science Basis. Contribution of Working Group I to the Fourth Assessment Report of the Intergovernmental Panel on Climate Change, edited by: Solomon, S., Qin, D., Manning, M., Chen, Z., Marquis, M., Averyt, K. B., Tignor, M., and Miller, H. L., 2007.
Richey, J. E., Mertes, L. A. K., Dunne, T., Victoria, R. L., Forsberg, B. R., Tancredi, A. C. N. S., and Oliveira, E.: Sources and routing of the Amazon River flood wave, Global Biogeochem. Cy., 3, 191–204, 1989.
Richey, J. E., Melack, J. M., Aufdenkampe, A. K., Ballester, V. M., and Hess, L. L.: Outgassing from Amazonian rivers and wetlands as a large tropical source of atmospheric CO_2, Nature, 416, 617–620, doi:10.1038/416617a, 2002.
Rost, S., Gerten, D., Bondeau, A., Lucht, W., Rohwer, J., and Schaphoff, S.: Agricultural green and blue water consumption and its influence on the global water system, Water Resour. Res., 44, W09405, doi:10.1029/2007wr006331, 2008.
Rowell, D. P.: Sources of uncertainty in future changes in local precipitation, Clim. Dynam., doi:10.1007/s00382-011-1210-2, in press, 2011.

HESSD
9, 261–300, 2012

Sampaio, G., Nobre, C., Costa, M. H., Satyamurty, P., Soares, B. S., and Cardoso, M.: Regional climate change over Eastern Amazonia caused by pasture and soybean cropland expansion, Geophys. Res. Lett., 34, L17709, doi:10.1029/2007GL030612, 2007.

Sitch, S., Smith, B., Prentice, I. C., Arneth, A., Bondeau, A., Cramer, W., Kaplan, J. O., Levis, S., Lucht, W., Sykes, M. T., Thonicke, K., and Venevsky, S.: Evaluation of ecosystem dynamics, plant geography and terrestrial carbon cycling in the LPJ dynamic global vegetation model, Global Change Biol., 9, 161–185, doi:10.1046/j.1365-2486.2003.00569.x, 2003.

Sitch, S., Huntingford, C., Gedney, N., Levy, P. E., Lomas, M., Piao, S. L., Betts, R., Ciais, P., Cox, P., Friedlingstein, P., Jones, C. D., Prentice, I. C., and Woodward, F. I.: Evaluation of the terrestrial carbon cycle, future plant geography and climate-carbon cycle feedbacks using five dynamic global vegetation models (DGVMs), Global Change Biol., 14, 2015–2039, doi:10.1111/j.1365-2486.2008.01626.x, 2008.

ter Steege, H., Pitman, N., Sabatier, D., Castellanos, H., Van der Hout, P., Daly, D. C., Silveira, M., Phillips, O., Vasquez, R., Van Andel, T., Duivenvoorden, J., De Oliveira, A. A., Ek, R., Lilwah, R., Thomas, R., Van Essen, J., Baider, C., Maas, P., Mori, S., Terborgh, J., Vargas, P. N., Mogollon, H., and Morawetz, W.: A spatial model of tree alpha-diversity and tree density for the Amazon, Biodivers. Conserv., 12, 2255–2277, doi:10.1023/A:1024593414624, 2003.

Wagner, W., Scipal, K., Pathe, C., Gerten, D., Lucht, W., and Rudolf, B.: Evaluation of the agreement between the first global remotely sensed soil moisture data with model and precipitation data, J. Geophys. Res., 108, 4611, doi:10.1029/2003JD003663, 2003.

Willmott, C. J.: Some comments on the evaluation of model performance, B. Am. Meteorol. Soc., 63, 1309–1313, 1982.

Wittmann, F., Junk, W. J., and Piedade, M. T. F.: The Várzea forests in Amazonia: flooding and the highly dynamic geomorphology interact with natural forest succession, Forest Ecol. Manage., 196, 199–212, doi:10.1016/j.foreco.2004.02.060, 2004.

Worbes, M.: The forest ecosystem of the floodplains, in: The Central Amazon Floodplain, edited by: Junk, W. J., Springer, Berlin, Germany, 223–265, 1997.

WWF HydroSHEDS: HydroSHEDS, http://hydrosheds.cr.usgs.gov/, last access: 15 October 2007.

HESSD
9, 261–300, 2012

Table 1. Slope classes.

Slope range	Class
≤ 1.5°	5
>1.5– ≤ 3°	4
>3– ≤ 6°	3
>6– ≤ 10°	2
>10– ≤ 35°	1
>35°	0

HESSD
9, 261–300, 2012

Table 2. Relative slope position classes.

Distance range	Class
0–10 cells	22
11–20 cells	19
21–40 cells	13
41–60 cells	12
61–80 cells	11
>81 cells	10

HESSD
9, 261–300, 2012

Table 3. Landform types with corresponding slope and mTRMI.

Landform type	Slope range	mTRMI
Valley flats	<3°	>22
Nearly level terraces	<3°	≤22
Gently sloping toe slopes, and bottoms	≥3– <10°	>18
Gently sloping ridges	≥3– <10°	≤18
Very moist steep slopes	≥10– ≤35°	≥18
Moderately moist steep slopes	≥10– ≤35°	11–17
Dry steep slopes	≥10– ≤35°	<10

HESSD
9, 261–300, 2012

Table 4. List of the 24 IPCC climate models used in this study. Details for the climate models see IPCC 2007 AR4, chapter 8 (Randall et al., 2007).

Model name	
BCCR – BCM 2.0	INGV – SXG
CCCMA – CGCM 3.1 (T47)	INM – CM 3.0
CCCMA – CGCM 3.1 (T63)	IPSL – CM 4
CNRM – CM 3	MIROC 3.2 (hires)
CSIRO – Mk 3.0	MIROC 3.2 (medres)
CSIRO – Mk 3.5	MIUB – ECHO-G
GFDL – CM 2.0	MPI – ECHAM 5
GFDL – CM 2.1	MRI – CGCM 2.3.2a
GISS – AOM	NCAR – CCSM 3
GISS – EH	NCAR – PCM 1
GISS – ER	UKMO – HadCM 3
FGOALS – g 1.0	UKMO – HadGEM 1

HESSD
9, 261–300, 2012

Table 5. Overview of the sites chosen to show detailed discharge validation.

Site	Coordinates	River	Obs. years	Obs. mean annual discharge (m^3)	Sim. mean annual discharge (m^3)	Willmotts' index of agreement	Error of qualitative validation
Cruzeiro do Sul	7.62° S 72.67° W	Rio Jurua	1967–1997	11 000	13 600	0.8797	0.263
Porto Velho	8.76° S 63.91° W	Rio Madeira	1969–1979	210 500	204 500	0.9318	0.094
Óbidos[a]	1.91° S 55.55° W	Rio Amazonas	1928–1995 [b]	1 870 000	1 759 000	0.8725; 0.9107 [a]	0.996; 0.994 [a]

[a] Data of two available sources; [b] gap between 1948 and 1968.

HESSD
9, 261–300, 2012

Table 6. Comparison of observed floodplain area and calculated floodable area in the subregions of the basin. *R* denotes the rectangle number in Fig. 5.

Source	*R*	North-West corner	South-East corner	Floodplain area (10^3 km^2)		Fraction (%)	
				published	calculated	published	calculated
Richey et al. (2002)	1	0°/72° W	8° S/54° W	290.0	239.5	16.3	13.5
Melack et al. (2004)	1	0°/72° W	8° S/54° W	190.3	239.5	10.7	13.5
Hamilton et al. (2002)	2	2° S/70° W	5° S/52° W	97.4	91.4	14.6	13.7
Hamilton et al. (2002)	3	12° S/68° W	16° S/61° W	92.1	49.4	27.4	14.7

HESSD
9, 261–300, 2012

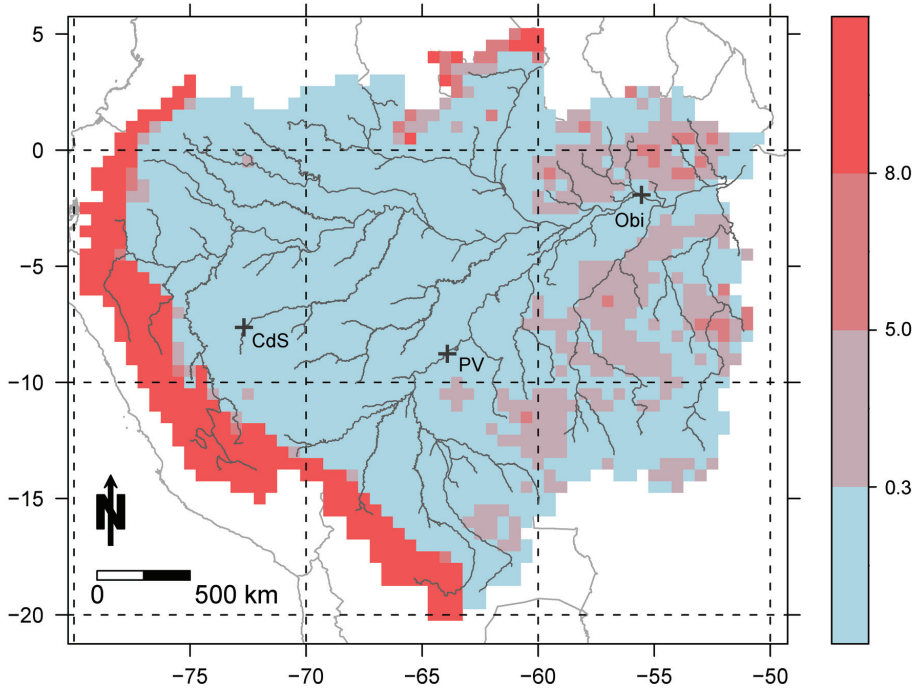

Fig. 1. Slope-dependent flow velocity ($m\,s^{-1}$) in the Amazon catchment, with river network shown in grey. The black crosses indicate the test sites Cruzeiro do Sul (CdS), Porto Velho (PV), and Óbidos (Obi).

HESSD
9, 261–300, 2012

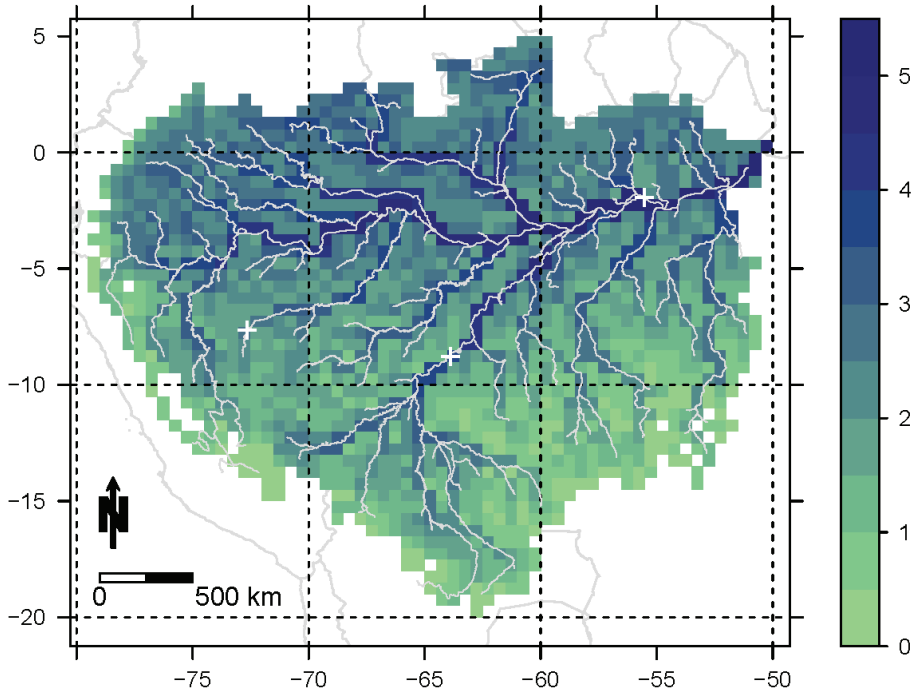

Fig. 2. Simulated mean discharge ($\log 10\,m^3\,s^{-1}$) during June, averaged over the reference period 1961–1990.

HESSD
9, 261–300, 2012

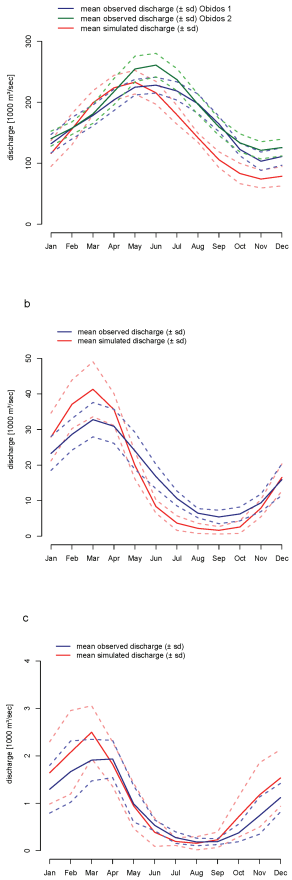

Fig. 3. Observed and simulated mean discharge ($10^3\,m^3\,s^{-1}$) for 1969 to 1979 (± standard deviation, shown as dashed lines) **(a)** for Óbidos station (note that for this station two sources for discharge data are available – ANEEL, blue, and Anonymous, green), **(b)** for Porto Velho station and **(c)** for Cruzeiro do Sul station.

HESSD
9, 261–300, 2012

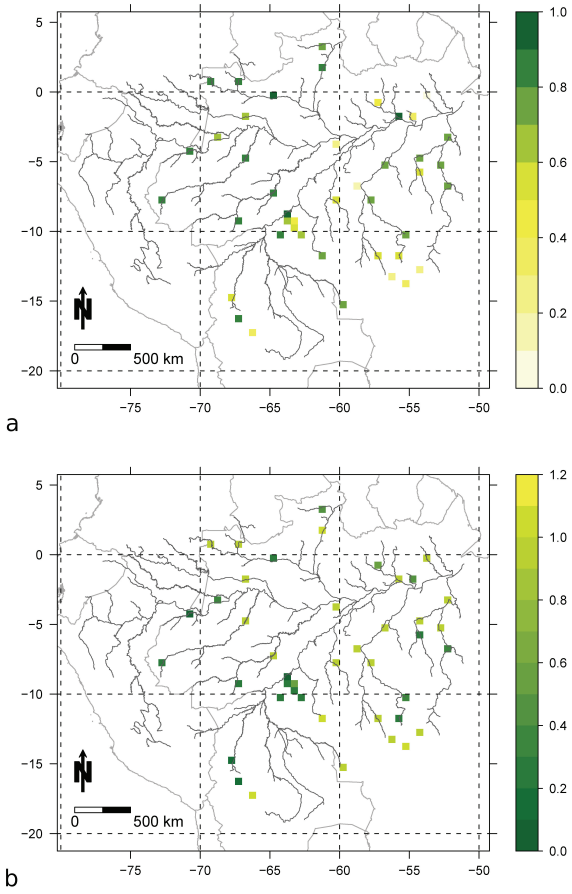

Fig. 4. Comparison of observed and simulated discharge for 45 observation sites with **(a)** Willmott's index of agreement (1.0 indicates complete agreement) and **(b)** error of the qualitative validation (0.0 indicates complete agreement).

HESSD
9, 261–300, 2012

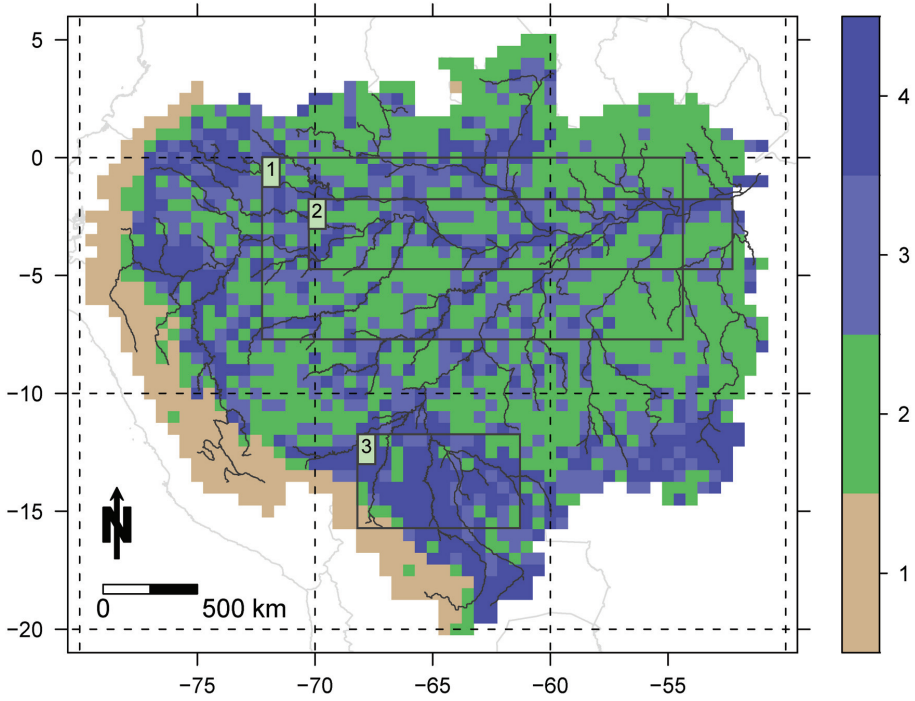

Fig. 5. Fraction classes of floodable area per cell. Class 1 representing 0–6 %, class 2 representing 7–13 %, class 3 representing 14 %, class 4 representing >14 % of floodable area. For a comparison of simulated floodable area with floodplain area (rectangles R1–R3) see Table 5.

HESSD
9, 261–300, 2012

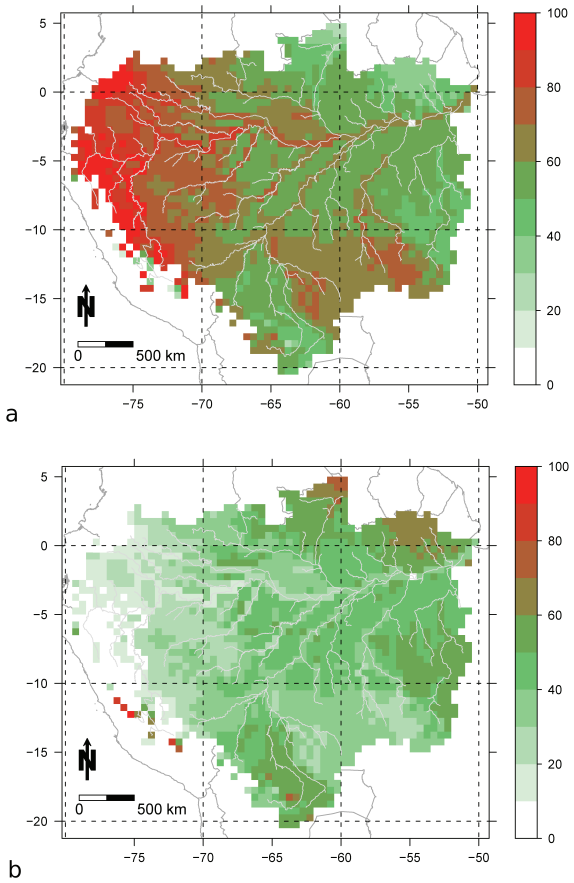

Fig. 6. Probability (%) of an increase **(a)** and a decrease **(b)** of mean annual inundated area per cell. The probability represents the agreements between the 24 model runs showing an increase or a decrease in inundated area, respectively.

HESSD
9, 261–300, 2012

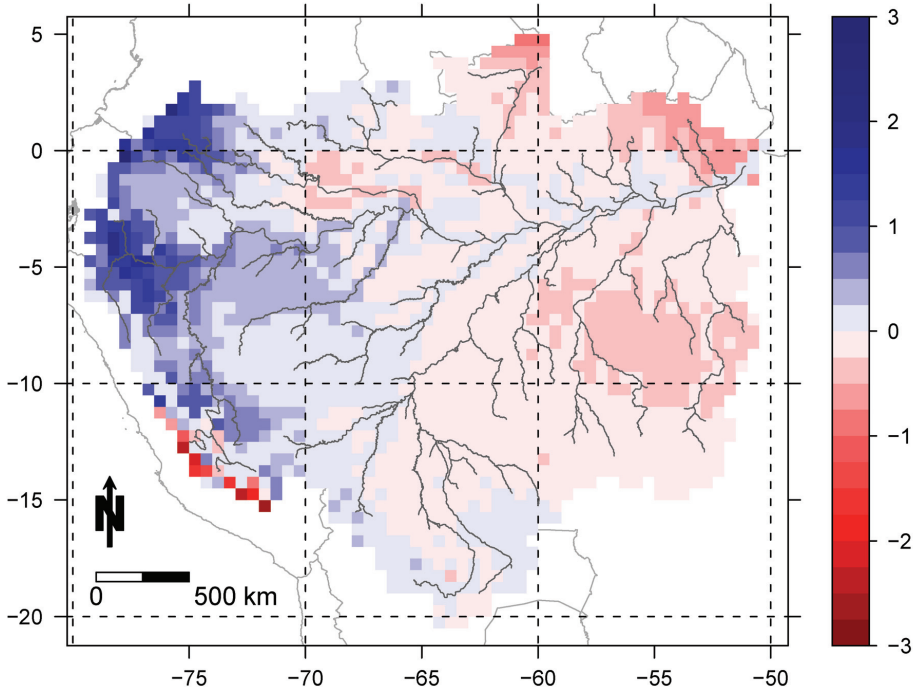

Fig. 7. Lengthening (blue) and shortening (red) of duration of inundation in months (mean over 24 model runs) between future and reference period.

HESSD
9, 261–300, 2012

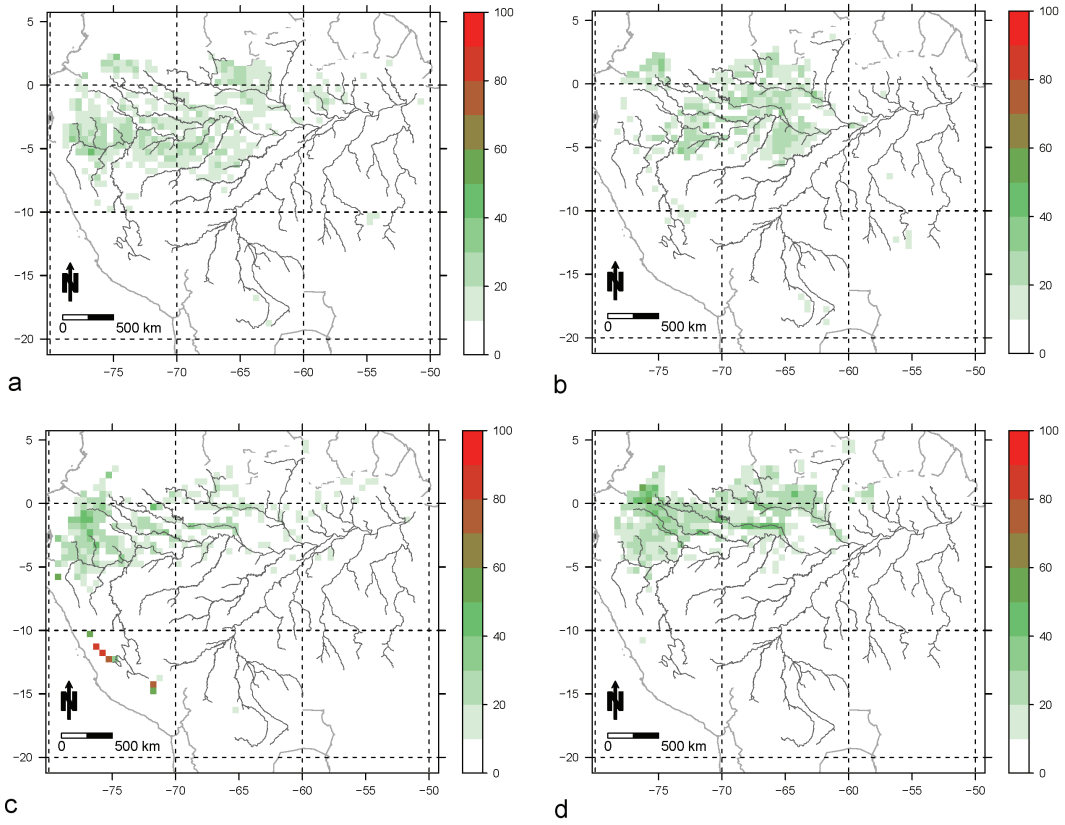

Fig. 8. Probability (%) of a forward shift **(a, c)** and backward shift **(b, d)** between future and reference period of at least 3-months of high water peak month **(a, b)** and low water peak month **(c, d)**.

HESSD
9, 261–300, 2012

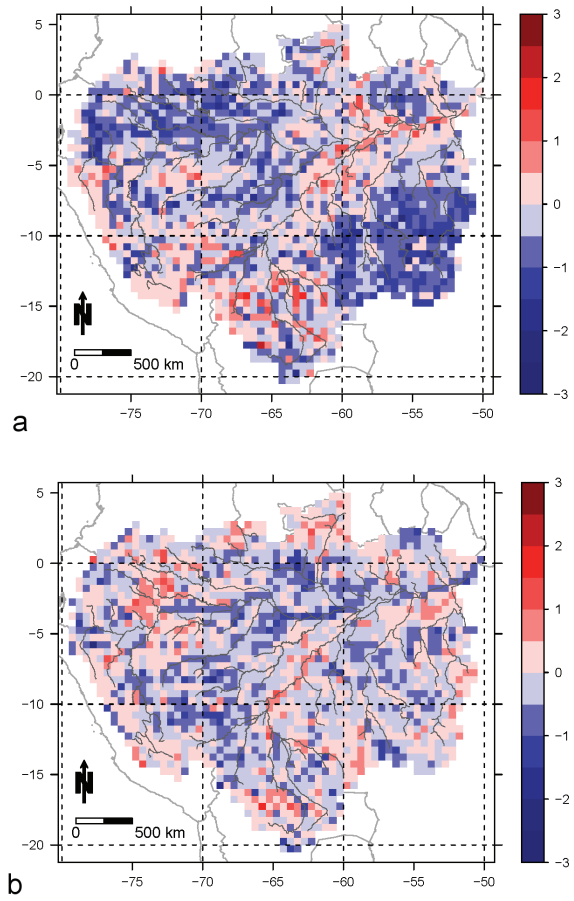

Fig. 9. Difference of the number of extremely dry years **(a)** and extremely wet years **(b)** between future and reference period.

HESSD
9, 261–300, 2012

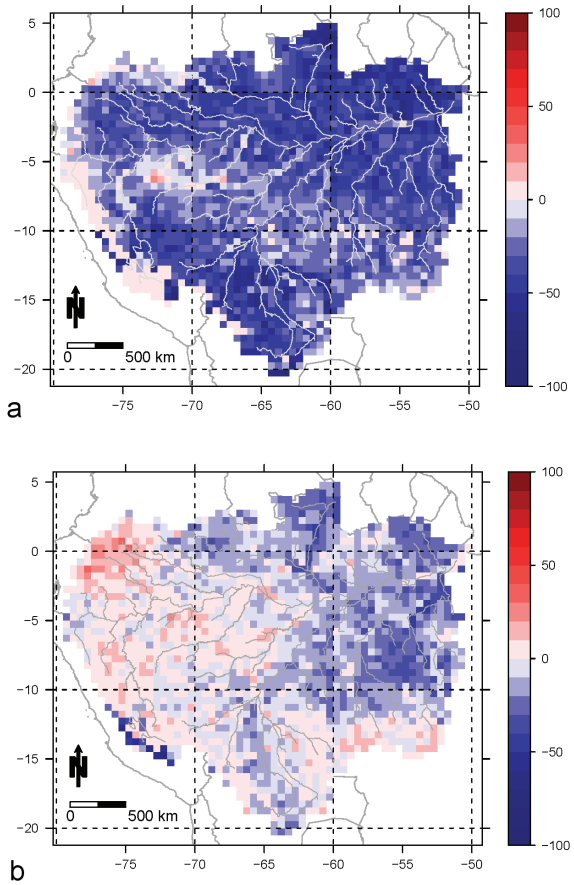

Fig. 10. Difference in the probability of at least three consecutive extremely dry years **(a)** and extremely wet years **(b)** between the future and reference period.

HESSD
9, 261–300, 2012